# Global distribution of wave amplitudes and wave normal angles of chorus waves using THEMIS wave observations

W. Li,[1] J. Bortnik,[1] R. M. Thorne,[1] and V. Angelopoulos[2]

Received 26 July 2011; revised 1 September 2011; accepted 22 September 2011; published 7 December 2011.

[1] The global distribution of chorus wave amplitudes and their wave normal angles is investigated using high-resolution wave spectra and waveform data from THEMIS for lower-band and upper-band chorus separately. Statistical results show that large amplitude chorus (>300 pT) occurs predominantly from premidnight to postdawn and is preferentially observed at lower L shells (<8) near the magnetic equator. However, strong or moderate chorus extends further into the afternoon sector and to higher L shells. For lower-band chorus, strong waves (>50 pT) tend to have wave normal angles of <20° and their wave normal angles become even smaller with increasing wave amplitudes. For modest waves, the wave normal angles are distributed over a broad range with a major peak at <20° and a secondary peak at 60°–80°. Wave normal angles of lower-band chorus are generally smaller on the dayside than on the nightside possibly due to the more uniform and more compressed magnetic field configuration on the dayside. Lower-band chorus becomes more oblique with increasing latitude on the dayside, whereas on the nightside the probability of observing oblique chorus decreases at higher latitudes. Compared to lower-band chorus, the properties of upper-band chorus are somewhat different. Upper-band chorus is considerably weaker in magnetic wave amplitudes, shows tighter confinement to the magnetic equator (<10°), and occurs at smaller L shells (<8). Furthermore, wave normal angles of upper-band chorus are generally larger than those of lower-band chorus, but the occurrence rate still peaks at wave normal angles of <20°, particularly for strong upper-band chorus.

**Citation:** Li, W., J. Bortnik, R. M. Thorne, and V. Angelopoulos (2011), Global distribution of wave amplitudes and wave normal angles of chorus waves using THEMIS wave observations, *J. Geophys. Res.*, *116*, A12205, doi:10.1029/2011JA017035.

## 1. Introduction

[2] Chorus emissions are very intense electromagnetic whistler mode waves, excited naturally in the low-density region outside the plasmapause [*Burtis and Helliwell*, 1969; *Tsurutani and Smith*, 1974; *Meredith et al.*, 2001, 2003]. The source region of chorus waves is generally believed to be located near the geomagnetic equator, and the waves subsequently propagate to higher latitudes in both the Northern and Southern Hemispheres [*LeDocq et al.*, 1998; *Lauben et al.*, 2002; *Santolík et al.*, 2003; *Bortnik et al.*, 2007a].

[3] Spacecraft observations show that chorus consists of discrete elements with rising or falling tones and sometimes short impulsive bursts [e.g., *Burtis and Helliwell*, 1969; *Burton and Holzer*, 1974; *Hayakawa et al.*, 1984; *Santolík et al.*, 2003; *Li et al.*, 2011]. The frequency of chorus emissions is closely related to the equatorial electron cyclotron frequency ($f_{ce}$), typically occurring in the frequency range 0.1–0.8 $f_{ce}$, where $f_{ce}$ is the equatorial electron cyclotron frequency [*Burtis and Helliwell*, 1969; *Tsurutani and Smith*, 1977; *Santolík et al.*, 2003]. Interestingly, chorus emissions are commonly observed in two distinct frequency bands (lower-band and upper-band) with minimum wave power near 0.5 $f_{ce}$ [*Tsurutani and Smith*, 1974; *Koons and Roeder*, 1990]. Previous studies have shown that nightside chorus waves are confined to within ~15° of the magnetic equator, whereas dayside chorus waves extend to higher magnetic latitudes [*Tsurutani and Smith*, 1977; *Meredith et al.*, 2003; *Li et al.*, 2009; *Bunch et al.*, 2011]. *Santolík et al.* [2005] investigated the radial evolution of chorus and showed that upper-band chorus is only excited at L shells below 8, whereas lower-band chorus can be observed at L shells up to 11–12.

[4] In addition to the important role of chorus waves in both the loss and acceleration processes of radiation belt electrons [e.g., *Lorentzen et al.*, 2001; *Horne et al.*, 2005a; *Thorne et al.*, 2005; *Chen et al.*, 2007; *Li et al.*, 2007; *Shprits et al.*, 2009; *Thorne*, 2010], large amplitude chorus has recently received more attention due to its pronounced nonlinear interaction with energetic electrons [e.g., *Albert*, 2002; *Bortnik et al.*, 2008]. *Bortnik et al.* [2008] demonstrated that

[1]Department of Atmospheric and Oceanic Sciences, University of California at Los Angeles, California, USA.
[2]Department of Earth and Space Sciences, Institute of Geophysics and Planetary Physics, University of California at Los Angeles, California, USA.


0148-0227/11/2011JA017035

low amplitude waves exhibit linear scattering, which leads to large-scale diffusive behavior, whereas large amplitude waves can result in monotonic decreases in pitch angle and energy, causing large-scale de-energization and particle loss. Therefore, they suggested that the intensity of individual, discrete chorus element is a critical parameter to measure in order to quantify the large-scale dynamics of the radiation belts.

[5] Using high time resolution wave data, recent observations [e.g., *Cattell et al.*, 2008; *Cully et al.*, 2008a] reported large amplitude whistlers, with amplitudes that are significantly larger than the typical time-averaged chorus wave amplitudes reported previously [*Meredith et al.*, 2003; *Horne et al.*, 2005b; *Li et al.*, 2009]. However, these reported large amplitude chorus waves are mostly individual events, and it is important to systematically investigate the occurrence rate and characteristics of chorus waves to quantitatively evaluate their role in radiation belt electron dynamics. The global distribution of chorus wave amplitudes was shown in *Li et al.* [2009] using filter bank data (averaged over 4 s) from THEMIS. However, this database is unable to capture large amplitude chorus bursts, which occur on typical time intervals that are less than a few tenths of second [e.g., *Cully et al.*, 2008a]. Furthermore, six frequency bands of the filter bank data over the frequency range of 4–4000 Hz are insufficient to accurately differentiate between lower-band and upper-band chorus, even though the typical characteristics of the two bands could be very different [e.g., *Hayakawa et al.*, 1984]. Therefore, the first objective of this paper is to investigate the global distribution of lower-band and upper-band chorus wave amplitudes, with particular emphasis on the properties of large amplitude chorus, using the wave data from the THEMIS spacecraft.

[6] The wave normal distribution is important for understanding the generation and propagation characteristics of chorus waves, as well as for quantitatively evaluating their effects on radiation belt electrons. Therefore, the distribution of chorus wave normal angles has been a subject of interest during the past a few decades. Previous studies of wave normal distributions of lower-band chorus showed some consistency near the equator. Using OGO 5 wave measurements, *Burton and Holzer* [1974] and *Goldstein and Tsurutani* [1984] found that the majority of lower-band chorus waves near the geomagnetic equator have wave normal angles within 20° of the background magnetic field. In addition, *Goldstein and Tsurutani* [1984] found a small concentration of wave normal angles near the Gendrin angle in the frequency range of 0.3–0.45 $f_{ce}$. More recently, using wave measurements from the Cluster satellites together with ray tracing, *Breneman et al.* [2009] reported that near the magnetic equator lower-band chorus is preferentially excited with wave normal angles either within 20° of the ambient magnetic field or near the Gendrin angle. Later, using wave data from the Polar spacecraft, *Haque et al.* [2010] found that for lower-band chorus wave normal angles less than 20° have the highest occurrence rate, with a secondary peak occurring near the Gendrin angle, in the latitude range of 10°–50°. *Santolík et al.* [2009] and *Chum et al.* [2009] showed very oblique lower-band chorus waves falling in frequency, with wave normal angles close to the resonance cone. More recently, *Li et al.* [2011] found that rising tone chorus is typically quasi-field-aligned, whereas falling tone chorus is predominantly very oblique. However, previous studies showed inconsistency in the latitudinal dependence of lower-band chorus wave normal angles. While *Breneman et al.* [2009] reported that the wave normal angles become more oblique as waves propagate from the equator toward higher latitudes, consistent with ray tracing results of whistler mode chorus waves [e.g., *Thorne and Kennel*, 1967; *Horne and Thorne*, 2003; *Li et al.*, 2008], *Haque et al.* [2010] found that the probability of quasi-field-aligned waves increases and the probability of oblique waves decreases with increasing latitudes.

[7] Wave normal analysis of upper-band chorus has led to widely divergent results, ranging from essentially field-aligned [*Hospodarsky et al.*, 2001; *Lauben et al.*, 2002] to highly oblique with wave normal angles close to the resonance cone [*Hayakawa et al.*, 1984; *Muto et al.*, 1987]. *Breneman et al.* [2009] reported that upper-band chorus is generally found at relatively larger wave normal angles between 30° and 40°. *Haque et al.* [2010] showed that for upper-band chorus, 50% of the wave normal angles at latitudes near the magnetic equator have values less than 10°, whereas the wave normal angles are close to the resonance cone for some other cases. *Haque et al.* [2010] also found that the probability of observing these larger wave normal angles of upper-band chorus decreases with increasing latitude.

[8] Despite the above reported studies, a general consensus has not been reached regarding chorus wave normal distributions and their dependence on L, MLT, and MLAT. Therefore, the second objective of this study is to evaluate the wave normal angle distribution for lower-band and upper-band chorus.

[9] In section 2, we describe the analysis of THEMIS wave data. Observational results including the global distribution of wave amplitudes and wave normal distributions are shown in section 3 for lower-band and upper-band chorus separately. In section 4, we summarize and further discuss the principal results of the present study.

## 2. THEMIS Wave Data Analysis

[10] The THEMIS spacecraft, consisting of five probes in near-equatorial orbits with apogees above 10 $R_E$ and perigees below 2 $R_E$ [*Angelopoulos*, 2008], are well situated to measure chorus emissions in the near-equatorial magnetosphere. The Search-Coil Magnetometer (SCM) [*Le Contel et al.*, 2008; *Roux et al.*, 2008] measures low-frequency magnetic field fluctuations and waves in three orthogonal directions over a frequency range from 0.1 Hz to 4 kHz. The Electric Field Instrument (EFI) provides waveforms in three orthogonal directions from DC up to 8 kHz [*Bonnell et al.*, 2008]. Over a 24 h orbit, high-resolution waveform data are available for ~43 s with a sampling frequency up to ~16 kHz. One set of waveform data normally lasts 6–8 s and several waveform data sets recorded each day are distributed widely between the perigee and the apogee during the fast survey [*Angelopoulos*, 2008]. The magnetic field waveforms collected from 1 June 2008 to 1 June 2011 are used to obtain the polarization properties of the chorus waves. Since 1 May 2010, high-resolution wave power spectra data (fff data) have been available during the fast survey, ~12 h per day, thus providing excellent data coverage. These new wave spectra data are obtained by averaging

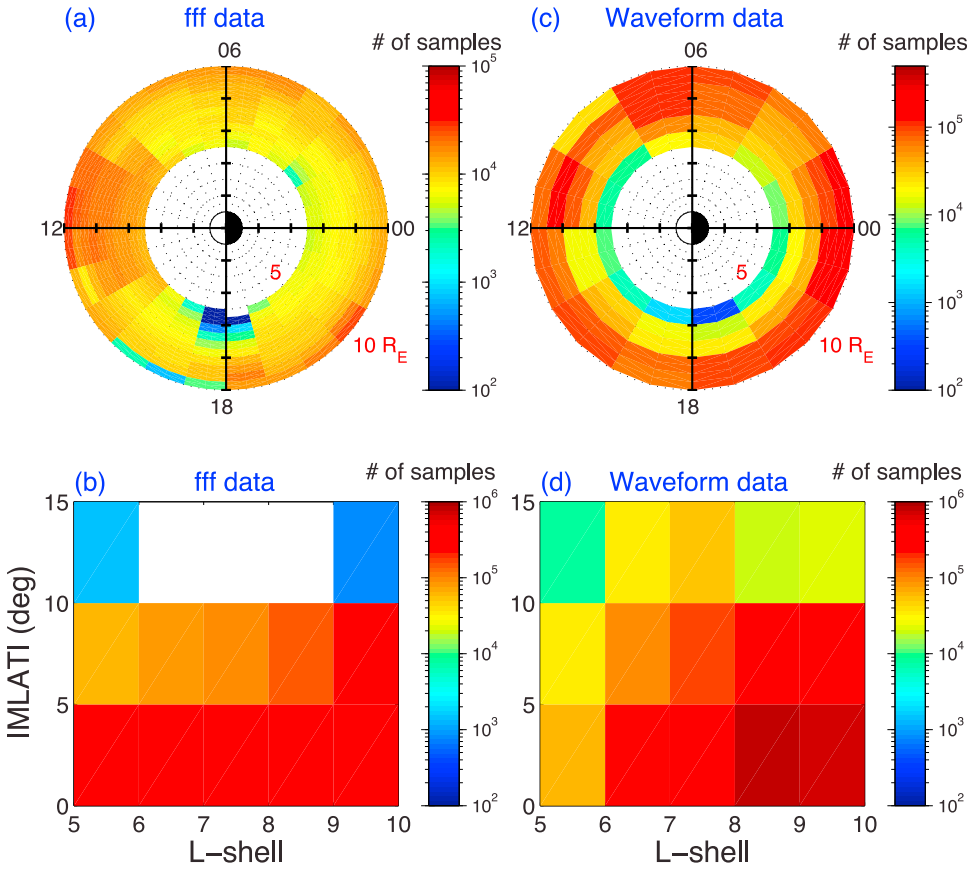


**Figure 1.** Global distribution of number of samples in (a) the L-MLT domain (0.5 L × 1 MLT) and (b) L-MLAT domain (1 L × 5 MLAT) obtained from fff data (1 May 2010 to 1 June 2011). Global distribution of number of samples in (c) the L-MLT domain (1 L × 2 MLT) and (d) L-MLAT domain (1 L × 5 MLAT) recorded during intervals when the waveform data are available (1 June 2008 to 1 June 2011). These data are collected in the region between 5 and 10 $R_E$ at all MLT.

spectra over 1 or 0.5 s and are recorded with a cadence of 8 s. Another advantage of this new data set is its high frequency resolution with 32 or 64 frequency bands logarithmically spaced over 4–4000 Hz [*Cully et al.*, 2008b], which is sufficient to differentiate lower-band and upper-band chorus. Therefore, fff magnetic wave spectra data collected between 1 May 2010 and 1 June 2011 are used to investigate the global distribution of wave amplitudes for lower-band and upper-band chorus separately. Magnetic wave amplitudes of chorus waves are obtained by integrating the magnetic field spectral density from fff data over 0.1–0.5 $f_{ce}$ and 0.5–0.8 $f_{ce}$ for lower-band chorus and upper-band chorus, respectively, since the majority of chorus wave power is confined to these frequency ranges [e.g., *Burtis and Helliwell*, 1969; *Tsurutani and Smith*, 1977; *Meredith et al.*, 2003]. The Fluxgate Magnetometer (FGM) [*Auster et al.*, 2008] measures the background magnetic fields and their low frequency fluctuations (up to 64 Hz). In this study, FGM data are utilized to evaluate local electron cyclotron frequencies in order to scale the chorus frequencies.

[11] Detailed wave polarization properties of chorus waves are obtained by analyzing three components of the wave magnetic field (converted into the magnetic field-aligned coordinate) from the waveform data using the method of *Bortnik et al.* [2007b] (essentially an implementation of *Means* [1972]). These calculated wave polarization properties have a time resolution of ~0.016 s, which is sufficient to capture the properties of each discrete chorus element, that typically lasts from ~0.1 s to a few tenths of seconds [e.g., *Cully et al.*, 2008a; *Santolík et al.*, 2008; *Macúšová et al.*, 2010]. Since we use only magnetic field components, there is a 180° ambiguity in the wave normal determination, and we converted all wave normal directions into values less than 90°. Polarization ratio ($R_p$) represents the ratio of polarized power to total power; ellipticity is defined as the ratio of the minor axis to the major axis in the plane perpendicular to the wave vector with a positive (negative) value corresponding to right-hand (left-hand) rotation about the wave vector [*Bortnik et al.*, 2007b]. For waves with sufficiently large values of the polarization ratio, which is the case for whistler mode chorus waves, the wave polarization method of *Bortnik et al.* [2007b] provides reliable polarization parameters (wave normal angle, azimuthal angle, ellipticity, etc). For each set of waveform data, we only recorded wave polarization parameters for waves with $R_p > 0.9$ and ellipticity >0.7, since chorus waves are normally highly polarized and are also nearly circularly right-hand polarized [e.g., *Tsurutani et al.*, 2009]. The observation is discarded if the recorded wave polarization parameters do not satisfy the above criteria. The wave polarization analysis for lower-band and upper-band chorus

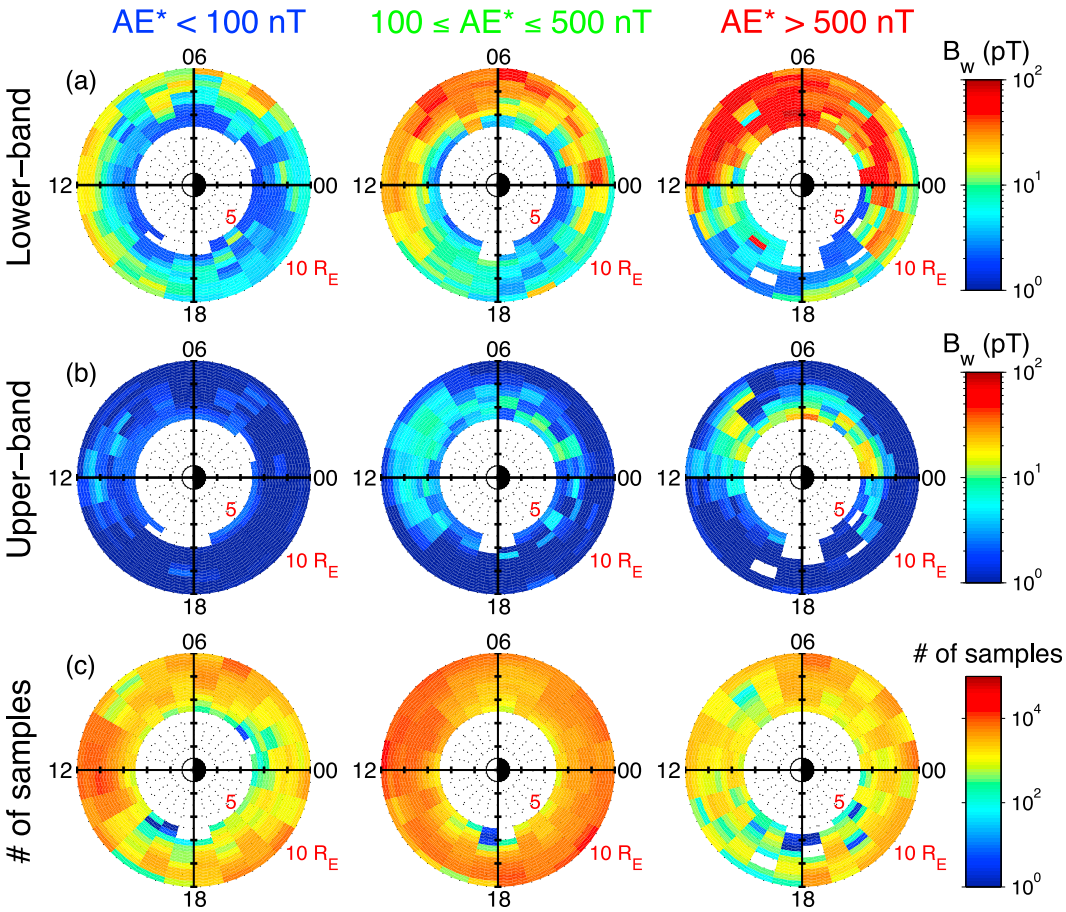


**Figure 2.** Global distribution of RMS magnetic wave amplitude from fff data at various levels of magnetic activity for (a) lower-band chorus and (b) upper-band chorus in each bin of 0.5 L × 1 MLT. (c) Number of samples under each corresponding magnetic activity level.

has been done separately for the corresponding frequency range of 0.1–0.5 $f_{ce}$ and 0.5–0.8 $f_{ce}$.

## 3. Observational Results

[12] The data set used in our statistical analysis includes two types of wave magnetic field data set, fff wave spectra data and waveform data. These data are collected from the three inner probes of THEMIS A, D, and E in the dominant chorus source region between 5 and 10 $R_E$ at all MLT. The fff data cover the period between 1 May 2010 and 1 June 2011 and waveform data cover a longer period from 1 June 2008 to 1 June 2011. We include waves observed outside the plasmapause and inside the magnetopause following the method by *Li et al.* [2010a] to exclude hiss waves and other magnetosheath emissions in our database.

[13] Figure 1 shows the number of samples regardless of the presence of chorus waves in L-MLT and L-MLAT domain for fff (Figures 1a and 1b) and waveform data (Figures 1c and 1d). The location parameters including L, MLT, and MLAT are obtained in the Solar Magnetic (SM) coordinate system for simplicity. Although fff data have been available since 1 May 2010, they provide excellent coverage in the dominant chorus source region between 5 and 10 $R_E$ at all MLT due to their high-percentage availability (~50%). Waveform data collected from the past three years also provide fairly good coverage in spite of their low-percentage availability (<~0.1%), as shown in Figures 1c and 1d. Since the THEMIS spacecraft are nearly equatorially orbiting satellites, the majority of data samples are confined to low magnetic latitudes, typically less than 20°, as shown in Figures 1b and 1d. We sort all samples obtained at $|\mathrm{MLAT}| > 10°$ into the bin between 10° and 15° due to the smaller number of data samples collected at $|\mathrm{MLAT}| > 10°$.

### 3.1. Global Distribution of Chorus Wave Amplitudes

[14] The global distribution of chorus magnetic wave amplitudes from fff data, categorized by various levels of AE* (the maximum AE in the previous 3 h), is shown in the L-MLT domain for lower-band (Figure 2a) and upper-band chorus (Figure 2b), respectively. The color bar indicates the root mean square (RMS) wave amplitudes in each 0.5 L × 1 MLT bin within the corresponding magnetic activity level. Note that periods with zero wave amplitudes (due the lack of chorus waves) are also used to calculate the RMS wave amplitudes, once they have been recorded under the corresponding magnetic activity levels. Figure 2c shows the number of samples recorded regardless of the presence of chorus waves in each corresponding category. Figures 2a and 2b show that wave amplitudes of both lower-band and upper-band chorus are observed from premidnight to the afternoon sector and generally dependent on magnetic

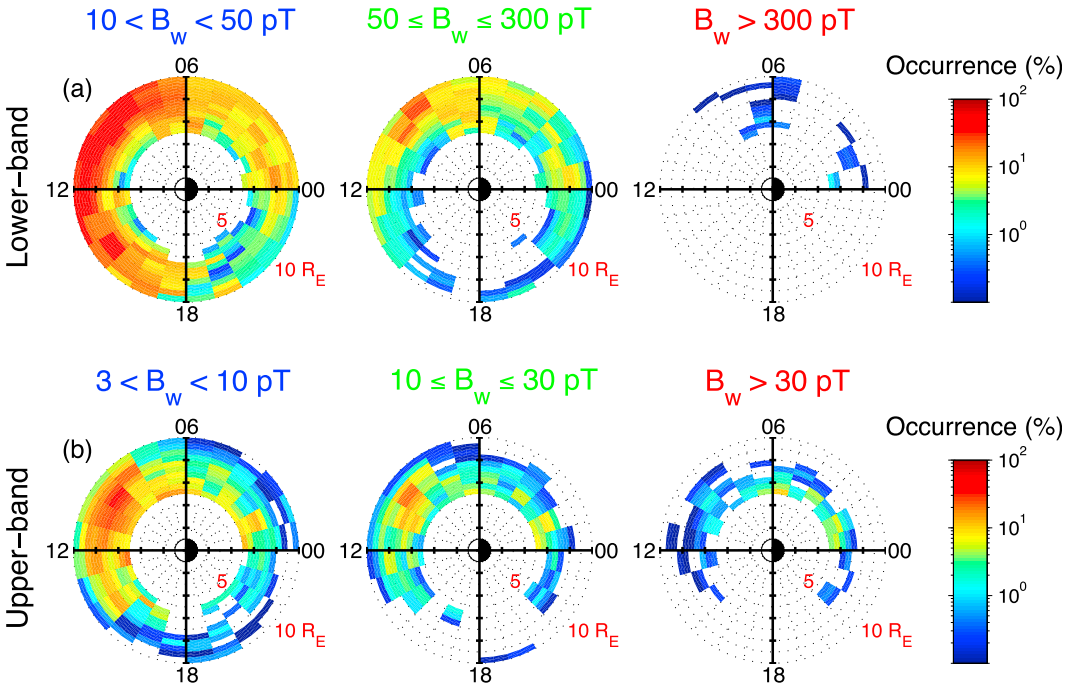


**Figure 3.** Global distribution of the occurrence rate of (a) lower-band chorus and (b) upper-band chorus for modest, strong, and large amplitude waves from fff data, shown in the L-MLT domain with a bin size of 0.5 L × 1 MLT.

activity, with larger wave amplitudes observed during stronger magnetic activity, consistent with previous studies by *Meredith et al.* [2003] and *Li et al.* [2009]. Interestingly, wave amplitudes near midnight are more closely related to AE*, since chorus wave generation near the midnight sector is directly relevant to substorm injection or enhanced convection. On the dayside, however, modest lower-band chorus is observed even during quite times (AE* < 100 nT). Furthermore, the preferential region of chorus generation tends to move closer to the Earth as the magnetic activity increases. Compared to lower-band chorus, upper-band chorus is much weaker and more confined to lower L shells (<8), consistent with *Santolík et al.* [2005]. This is probably because the generation of the upper-band chorus requires higher anisotropy of resonant electrons [e.g., *Kennel and Petschek*, 1966], which is preferentially present at lower L shells [*Li et al.*, 2010b].

[15] Figure 3 shows the global distribution of occurrence rates for various levels of chorus wave amplitude obtained from fff data in the L-MLT domain for lower-band (Figure 3a) and upper-band chorus (Figure 3b). Here the occurrence rate in each bin is defined as the ratio between the number of chorus wave events in each range of wave amplitudes and the total number of samples recorded regardless of the presence of chorus waves. The occurrence rate of the large amplitude ($B_w$ > 300 pT) lower-band chorus is extremely small, probably due to the insufficient time resolution of fff wave spectra data (averaged over 0.5 or 1 s), which may not necessarily capture discrete chorus elements. Strong lower-band chorus waves (50 ≤ $B_w$ ≤ 300 pT) indicate a moderate occurrence rate between midnight and noon up to ~20%. However, modest chorus waves (10 < $B_w$ < 50 pT) are distributed over a broad MLT range from the premidnight through dawn to the dusk sector with a much higher occurrence rate (up to ~50%). Note that the occurrence rate of modest lower-band chorus on the dayside is significantly higher than that on the nightside, consistent with *Li et al.* [2009]. Since the wave amplitude of upper-band chorus is generally much weaker than that of lower-band chorus, upper-band chorus is categorized by wave amplitude ranges different from those of lower-band chorus. Strong upper-band chorus ($B_w$ > 30 pT) is preferentially observed from premidnight to dawn, with an occurrence rate up to a few percent. Weak upper-band chorus (3 < $B_w$ < 10 pT), however, is more frequently observed on the dayside than on the nightside. This may suggest that generation of the strong upper-band chorus requires a relatively large resonant electron flux, which is found preferentially on the nightside [*Bortnik et al.*, 2007a; *Li et al.*, 2010b].

[16] In order to statistically investigate the preferential region of large amplitude chorus waves, we use the high-resolution waveform data from 1 June 2008 to 1 June 2011 from three inner THEMIS spacecraft to obtain chorus magnetic wave amplitude. Figure 4 shows the occurrence rate of large amplitude ($B_w$ > 300 pT) lower-band chorus in the L-MLT and L-MLAT domain. The occurrence rate is relatively high (up to a few percent) from premidnight to postdawn, probably because the resonant electron flux is typically larger on the nightside than on the dayside [e.g., *Bortnik et al.*, 2007a; *Li et al.*, 2010b]. Furthermore, large amplitude chorus waves are preferentially observed at lower L shells, where electron anisotropy of resonant electrons is higher [e.g., *Li et al.*, 2010b]. They also tend to be observed at lower magnetic latitudes, close to the generation region, probably because the waves experience strong attenuation due to Landau damping as they propagate to higher latitudes,

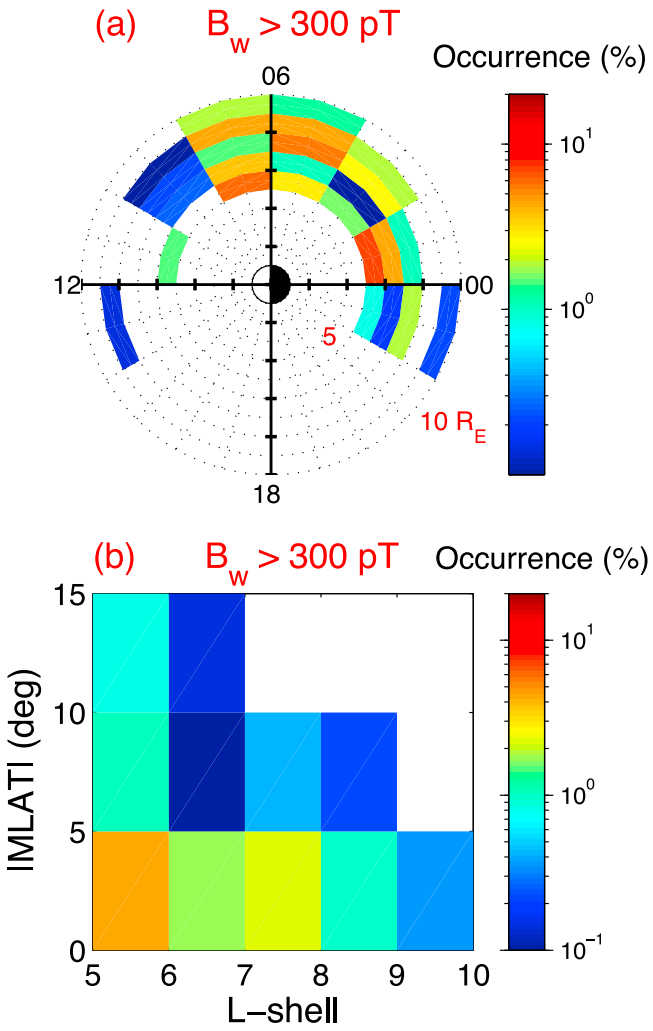


**Figure 4.** Global distribution of the occurrence rate of large amplitude lower-band chorus ($B_w$ > 300 pT) in (a) the L-MLT domain (1 L × 2 MLT) and (b) the L-MLAT domain (1 L × 5 MLAT), obtained using waveform data.

where their wave normal angles become more oblique. The occurrence rate of large amplitude chorus (>300 pT) obtained using waveform data (Figure 4a) is larger than that obtained from fff data (Figure 3, top right). This also confirms that high-resolution waveform data are needed to capture large amplitude chorus, which exhibits in discrete elements lasting less than a few tenths of seconds.

### 3.2. Wave Normal Distribution of Chorus Waves

[17] Wave normal angles of chorus waves are calculated from waveform data for lower-band and upper-band chorus separately. Figure 5 shows an example of chorus emissions from one set of waveform data observed by THEMIS E. Lower-band chorus exhibits discrete rising tones with a large magnetic wave amplitude up to ~1 nT (Figure 5c), whereas upper-band chorus shows hiss-like structure with a much weaker amplitude (<10 pT). For both lower-band and upper-band chorus, the polarization ratio (Figure 5e) is mostly larger than 0.9 and the ellipticity (Figure 5f) is higher than 0.7, indicating that these emissions exhibit typical features of whistler mode chorus waves. For these large amplitude lower-band chorus waves, the wave normal angles (Figure 5d) are mostly smaller than 20°, whereas the weak upper-band chorus is more oblique with the wave normal angles up to ~60°.

[18] In the following statistical results, all available waveform data are merged from 5 to10 $R_E$ and sorted into nightside (18–06 MLT) and dayside (06–18 MLT), indicated by blue and red bars, respectively, to investigate the latitudinal and MLT dependence of the wave normal distribution. Figure 6 shows wave normal distribution of lower-band and upper-band chorus, sorted into three designated amplitude ranges. The occurrence rate, defined as the ratio between the number of chorus wave events in each wave normal angle bin and the total number of chorus wave events in each wave amplitude level, is calculated separately on the nightside and dayside. Here one chorus wave event is defined as one set of chorus properties recorded with time resolution of ~0.016 s, satisfying the criteria described in section 2. For example, in Figure 6a, the values of 93,294 and 282,374 represent the total number of chorus events with wave amplitudes of 10 < $B_w$ < 50 pT on the nightside and dayside, respectively. For both lower-band and upper-band chorus, larger amplitude waves tend to have smaller wave normal angles than weaker waves. For lower-band chorus, more than ~80% of strong chorus (>50 pT) have wave normal angles <20°. However, for modest lower-band chorus (Figure 6a), the wave normal angles are distributed over a broad range (from 0° up to 80°) with a major peak at <20° and a small secondary peak at 60°–80°, which appears to be consistent with previous studies showing that most lower-band chorus have wave normal angles within 20° [e.g., *Goldstein and Tsurutani*, 1984; *Breneman et al.*, 2009]. For lower-band chorus, the wave normal angles are generally smaller on the dayside than on the nightside. This is consistent with expectation, since dayside chorus is more likely to stay field-aligned due to the more uniform and more compressed magnetic field configuration. Comparison of wave normal angles between lower-band and upper-band chorus indicates that the wave normal angle of upper-band chorus is generally larger than that of lower-band chorus. Note that we used slightly lower wave amplitude ranges for upper-band chorus in Figure 6 compared to those in Figure 3, since the number of samples of strong upper-band chorus with wave amplitudes larger than 30 pT is very limited from the waveform data. But it nevertheless is reasonable to show the main trend of wave normal distribution in various wave amplitude ranges. Similar occurrence rates are observed in the wave normal range of 0°–60° for both weak (Figure 6d) and modest upper-band chorus (Figure 6e), with a small peak at 10°–20°. However, for the strong upper-band chorus (Figure 6f), the dominant peak occurrence rate is observed over a 10°–20° wave normal range, with a small occurrence rate at wave normal angles larger than ~30°. Furthermore, a clear day-night dependence of the wave normal distribution is not observed for upper-band chorus.

[19] In Figure 7 we further sort wave normal distributions into three magnetic latitude ranges for all events recorded as lower-band and upper-band chorus. On the dayside, lower-band chorus shows a clear trend of increasing wave normal angles from lower to higher magnetic latitudes, which is likely caused by propagation in a heterogeneous medium,

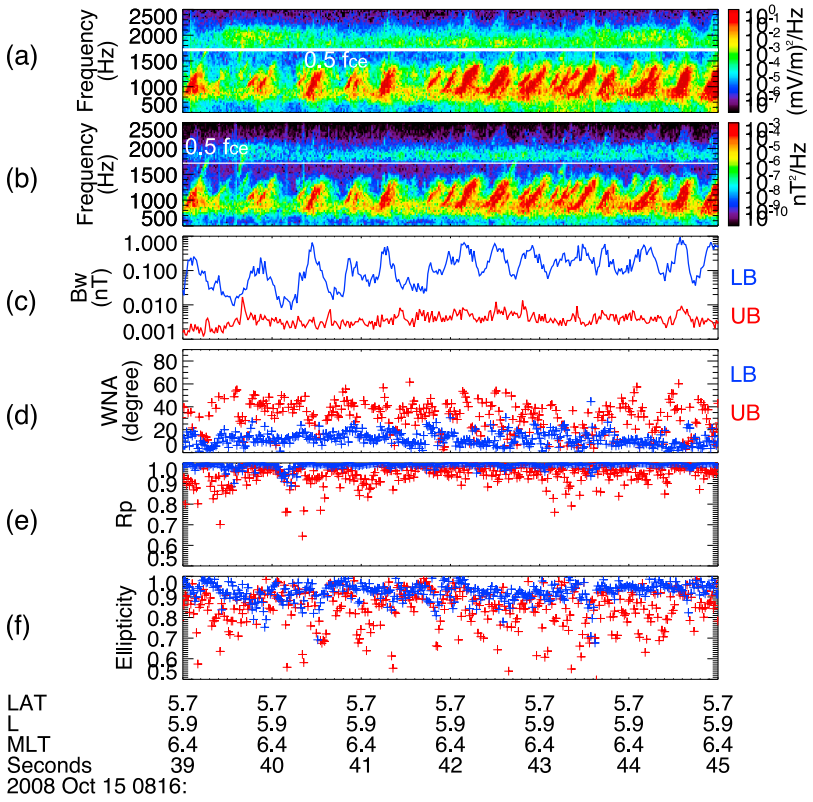


**Figure 5.** An example of chorus emissions from the waveform data observed by THEMIS E. Frequency-time spectrogram of wave spectral density in (a) electric field and (b) magnetic field, where the white solid line represents half of the equatorial electron cyclotron frequency. (c) Wave amplitudes of the lower-band (blue) and the upper-band (red) chorus, calculated through integrating wave magnetic field spectral density over the frequency range of 0.1–0.5 $f_{ce}$ and 0.5–0.8 $f_{ce}$. (d–f) Wave normal angle, polarization ratio, and ellipticity for the lower-band (blue) and the upper-band (red) chorus, respectively.

consistent with previous ray tracing results [e.g., *Thorne and Kennel*, 1967; *Horne and Thorne*, 2003; *Li et al.*, 2008] and observation [e.g., *Breneman et al.*, 2009]. Interestingly, the second peak around the wave normal angle of 70°–80° (Figure 7c) may reflect very oblique falling tones preferentially observed at higher latitudes ($|\mathrm{MLAT}| > 10°$) on the dayside [*Li et al.*, 2011]. At $|\mathrm{MLAT}| \geq 10°$ on the nightside, very few lower-band chorus waves (1013 out of 28,993) are recorded, which suggests that lower-band chorus may be extinguished efficiently as they propagate from lower to higher latitudes on the nightside. This is probably due to severe Landau damping, which becomes particularly important for oblique waves on the nightside. Therefore, most nightside chorus waves observed at relatively higher latitudes ($|\mathrm{MLAT}| > 10°$) have relatively small wave normal angles (<30°), and those with larger wave normal angle are probably attenuated due to Landau damping, consistent with *Haque et al.* [2010]. Near the geomagnetic equator ($|\mathrm{MLAT}| < 5°$), the occurrence rate of lower-band chorus peaks at wave normal angles of <20°, with a small secondary peak at large wave normal angles of 60°–70°. These large wave normal angles are observed very close to the equator, suggesting that those chorus waves are generated with oblique angles, consistent with previous studies [e.g., *Goldstein and Tsurutani*, 1984; *Breneman et al.*, 2009]. Compared to lower-band chorus, the wave normal distribution of upper-band chorus is generally more oblique and ranges from field-aligned to very oblique wave normal angles. At higher magnetic latitudes ($|\mathrm{MLAT}| > 10°$), no upper-band chorus is observed on the nightside and only 671 (out of 111,528) upper-band chorus events are observed on the dayside, indicating even stronger confinement to the geomagnetic equator than lower-band chorus. The more oblique upper-band chorus results in tighter confinement to the magnetic equator, probably due to the stronger Landau damping experienced by oblique waves.

## 4. Summary and Discussion

[20] We used high-resolution wave spectra data (fff) and waveform data from the THEMIS spacecraft to investigate the global distribution of wave amplitudes and wave normal angles and their dependence on MLAT, MLT, and L shells for lower-band and upper-band chorus separately. The principal findings of this study can be summarized as follows.

[21] 1. Wave amplitudes of both lower-band and upper-band chorus are activity dependent, generally having larger wave amplitudes during periods of stronger magnetic activity. Chorus wave amplitudes show a particularly close relation with AE* (maximum AE during the previous 3 h) on the nightside, where chorus generation is directly related to substorm injection or enhanced convection.

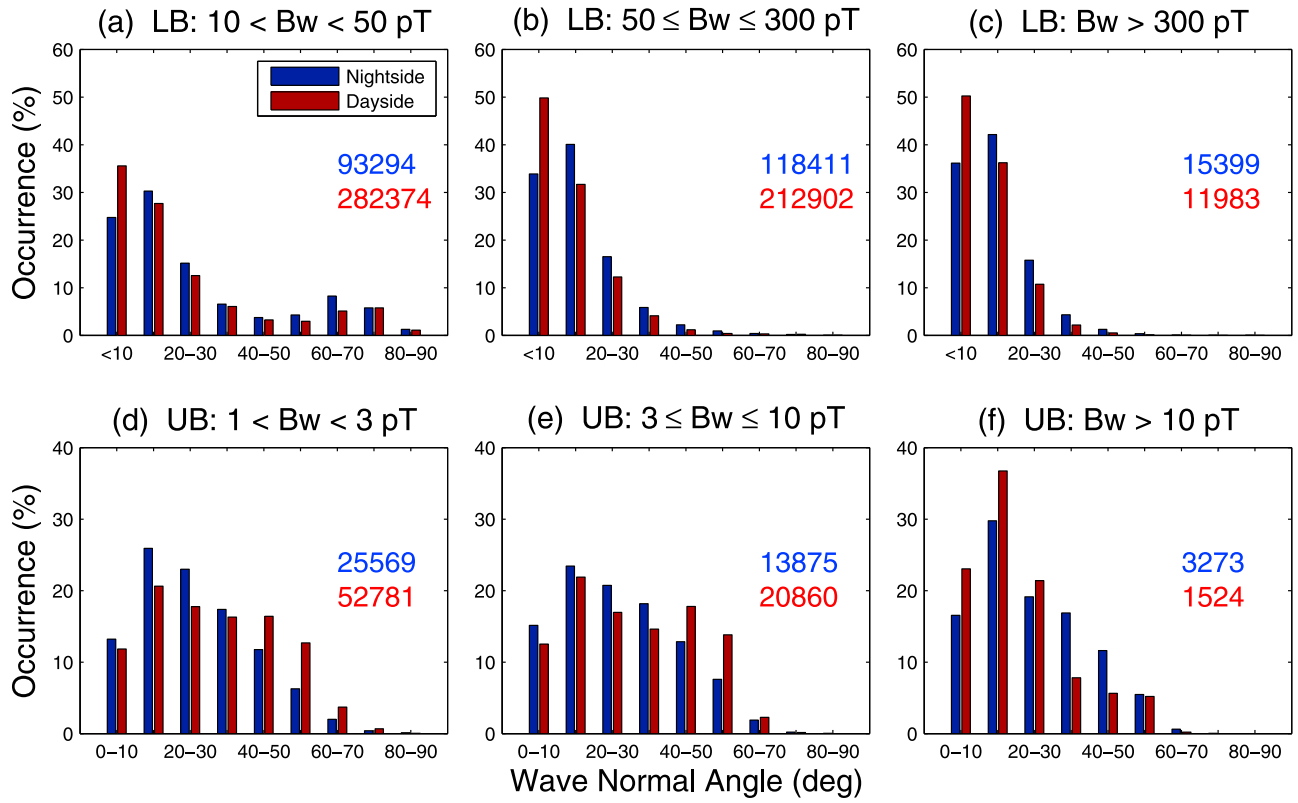


**Figure 6.** (a–c) Occurrence rates of various wave normal angles for different levels of wave amplitudes on the nightside (blue) and the dayside (red) for lower-band chorus. (d–f) Parameters as in (a–c) but for upper-band chorus. The numbers in each plot indicate the total number of chorus events collected from the nightside (blue) and the dayside (red), which are used to calculate the occurrence rate in each corresponding category.

[22] 2. For lower-band chorus, large amplitude (>300 pT) waves are typically observed from premidnight to postdawn near the magnetic equator with an occurrence rate up to a few percent, whereas weaker chorus extends through the noon to the dusk sector. In addition, large amplitude chorus is preferentially observed at lower L shells (<8).

[23] 3. For lower-band chorus, strong waves (>50 pT) tend to have small wave normal angles <20°. For modest waves, the wave normal angles are distributed over a broad range with a major peak at <20° and a small secondary peak at 60°–80°. The wave normal angles are generally smaller on the dayside than on the nightside, probably due to the more uniform and more compressed magnetic field configuration on the dayside. On the dayside, wave normal angles of lower-band chorus tend to increase from lower to higher magnetic latitudes, whereas on the nightside very few lower-band chorus waves are observed at high latitudes ($|\mathrm{MLAT}| > 10°$), generally having relatively small wave normal angles (<30°).

[24] 4. Characteristics of upper-band chorus are to some extent different from those of lower-band chorus. We summarize their differences as follows. Compared to lower-band chorus, the wave amplitude of upper-band chorus is considerably weaker. Upper-band chorus is confined to lower L shells (<8) and lower magnetic latitudes ($|\mathrm{MLAT}| < 10°$). Furthermore, the wave normal angles of upper-band chorus are generally larger than those of lower-band chorus, ranging from field-aligned to very oblique. For strong upper-band chorus, however, the wave normal occurrence rate still peaks at <20°. We suggest that the more oblique upper-band chorus is confined to lower magnetic latitudes possibly due to stronger Landau damping.

[25] In the present study, fff wave spectra data with high frequency resolution have been used to investigate the global distribution of chorus wave amplitudes for lower-band and upper-band chorus separately, which was not possible previously in *Li et al.* [2009] using THEMIS filter bank data. Note that our definition of wave amplitude is based only on its magnetic amplitude, which is commonly used to represent the intensity of the wave magnitude in calculating diffusion coefficients or test particle simulations [e.g., *Glauert and Horne*, 2005; *Bortnik et al.*, 2008; *Tao et al.*, 2011]. More importantly, we have used waveform data of the magnetic field from the three inner THEMIS spacecraft over ~3 years. While high-resolution waveform data provide limited statistics due to their low-percentage availability, they nevertheless cover the chorus dominant source region near the equator fairly well. High-resolution waveform data also allow us to capture large amplitude chorus, which occurs within a short time interval less than a few tenths of second. Furthermore, THEMIS waveform data provide detailed wave polarization properties, including wave normal angles and ellipticity, which are essential to understand the characteristics

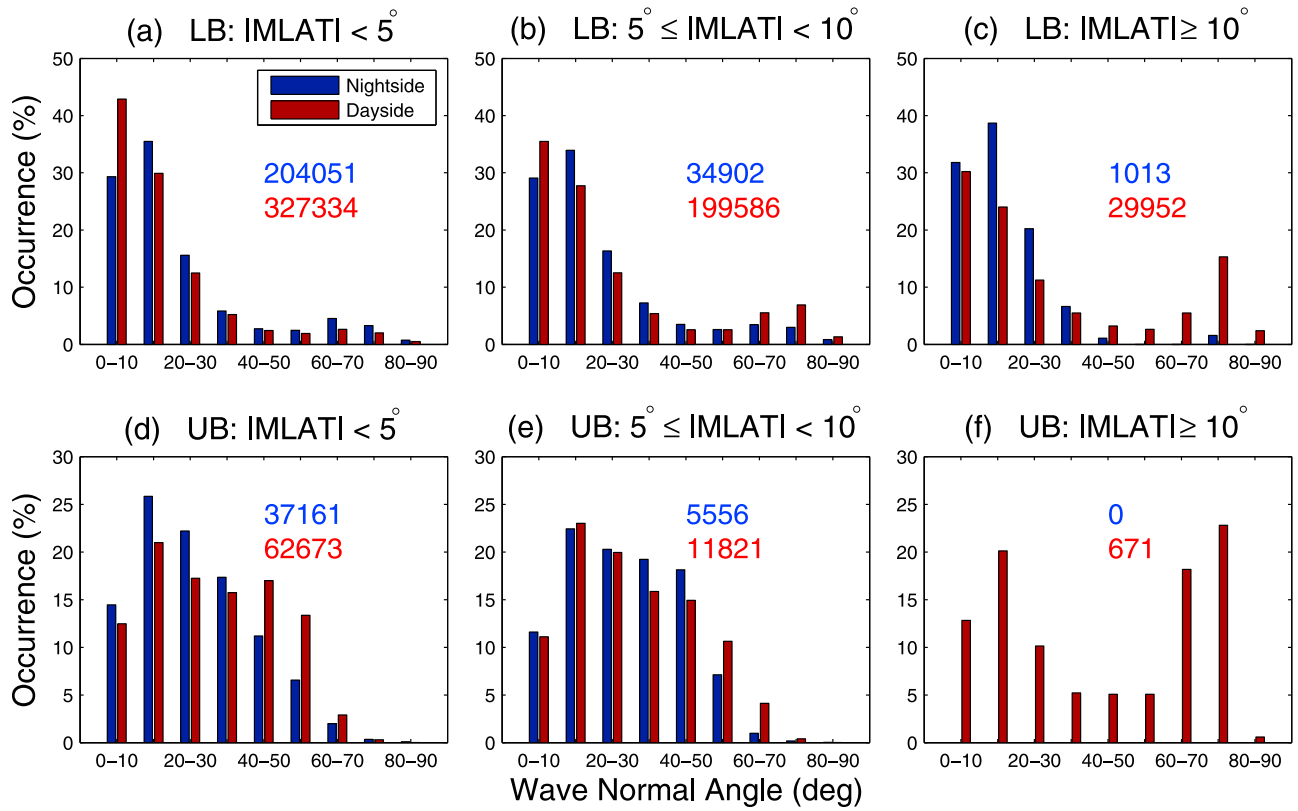


**Figure 7.** (a–c) The occurrence rates of various wave normal angles for different levels of magnetic latitudes on the nightside (blue) and the dayside (red) for lower-band chorus. (d–f) Parameters as in (a–c) but for upper-band chorus. The numbers in each plot indicate the total number of chorus events collected from the nightside (blue) and the dayside (red) in each corresponding category.

and propagation properties of chorus waves and are key parameters in calculating diffusion coefficients to evaluate the role of chorus waves in radiation belt electron dynamics.

[26] In previous studies of the latitudinal dependence of lower-band chorus, wave normal angle distribution showed somewhat divergent results [e.g., *Breneman et al.*, 2009; *Haque et al.*, 2010]. Using 52 chorus events from one orbit pass of the Cluster spacecraft at ~13 MLT and L shells of 5.6 to 4.9, *Breneman et al.* [2009] reported that chorus wave normal angles increase from lower to higher magnetic latitude, whereas by merging all available MLT and L shells from Polar wave data *Haque et al.* [2010] found that the detected chorus waves tend to become more field-aligned with increasing latitudes. By separating dayside from nightside chorus emissions, our results show that the latitudinal dependence of the wave normal distribution differs on the dayside and the nightside. The wave normal angles of the dayside chorus tend to become larger with increasing magnetic latitude, whereas on the nightside the majority of the chorus waves are found to be quasi-field-aligned (<30°) at $|\mathrm{MLAT}| > 10°$. We suggest that on the dayside, where the Landau damping is weaker due to the lower resonant electron fluxes [e.g., *Bortnik et al.*, 2007a; *Li et al.*, 2010b], chorus waves remain above the observable level due to less severe Landau damping, although they become more oblique when propagating from lower to higher latitudes, which is consistent with ray tracing results of whistler mode chorus [e.g., *Thorne and Kennel*, 1967; *Horne and Thorne*, 2003; *Li et al.*, 2008]. On the nightside, however, oblique chorus waves are probably efficiently attenuated and thus are below the observable level due to the severe Landau damping, and only chorus waves with small wave normal angles remain detectable at higher latitudes.

[27] Previous studies showed inconsistent wave normal distributions of upper-band chorus waves, ranging from predominantly field-aligned [*Hospodarsky et al.*, 2001; *Lauben et al.*, 2002; *Haque et al.*, 2010], relatively large wave normal angles between 30° and 40° [*Breneman et al.*, 2009], to highly oblique angles close to the resonance cone [*Hayakawa et al.*, 1984; *Muto et al.*, 1987]. Our results show that the wave normal distribution ranges widely from 0° to ~70° with a peak occurrence rate at 10°–20°, but the wave normal angles are predominantly quasi-field-aligned (<20°) for the strong upper-band chorus. Furthermore, one clear feature of the upper-band chorus from the present paper is that their wave normal angles are generally larger than those of lower-band chorus.

[28] An important aspect of this study is the comprehensive database on the large amplitude chorus waves, which probably play an important role in radiation belt electron dynamics due to their distinctive nonlinear interaction [e.g., *Bortnik et al.*, 2008]. Our results show that large amplitude chorus waves are preferentially observed at lower magnetic latitudes ($|\mathrm{MLAT}| < 10°$) from premidnight to postdawn

and the corresponding wave normal angles are typically quasi-field-aligned (<20°). These key features of the large amplitude chorus are crucial for evaluating the nonlinear effect of such chorus on radiation belt electrons.

[29] **Acknowledgments.** This research was funded in part by NASA grants NNX11AD75G, NNX08AI35G, and NAS5–02099, and NSF grant AGS-0840178. The authors acknowledge O. Le Contel and A. Roux for use of SCM data; J. W. Bonnell and F. S. Mozer for use of EFI data; and K. H. Glassmeier, U. Auster, and W. Baumjohann for the use of FGM data provided under the lead of the Technical University of Braunschweig and with financial support through the German Ministry for Economy and Technology and the German Center for Aviation and Space (DLR) under contract 50 OC 0302. We also thank the World Data Center for Geomagnetism, Kyoto, for providing the *AE* index.

[30] Robert Lysak thanks Eva Macúšová for her assistance in evaluating this paper.

## References

Albert, J. M. (2002), Nonlinear interaction of outer zone electrons with VLF waves, *Geophys. Res. Lett.*, *29*(8), 1275, doi:10.1029/2001GL013941.

Angelopoulos, V. (2008), The THEMIS Mission, *Space Sci. Rev.*, *141*(1–4), 5–34, doi:10.1007/s11214-008-9336-1.

Auster, H. U., et al. (2008), The THEMIS fluxgate magnetometer, *Space Sci. Rev.*, *141*(1–4), 235–264, doi:10.1007/s11214-008-9365-9.

Bonnell, J. W., F. S. Mozer, G. T. Delory, A. J. Hull, R. E. Ergun, C. M. Cully, V. Angelopoulos, and P. R. Harvey (2008), The Electric Field Instrument (EFI) for THEMIS, *Space Sci. Rev.*, *141*(1–4), 303–341, doi:10.1007/s11214-008-9469-2.

Bortnik, J., R. M. Thorne, and N. P. Meredith (2007a), Modeling the propagation characteristics of chorus using CRRES suprathermal electron fluxes, *J. Geophys. Res.*, *112*, A08204, doi:10.1029/2006JA012237.

Bortnik, J., J. W. Cutler, C. Dunson, and T. E. Bleier (2007b), An automatic wave detection algorithm applied to Pc1 pulsations, *J. Geophys. Res.*, *112*, A04204, doi:10.1029/2006JA011900.

Bortnik, J., R. M. Thorne, and U. S. Inan (2008), Nonlinear interaction of energetic electrons with large amplitude chorus, *Geophys. Res. Lett.*, *35*, L21102, doi:10.1029/2008GL035500.

Breneman, A. W., C. A. Kletzing, J. Pickett, J. Chum, and O. Santolík (2009), Statistics of multispacecraft observations of chorus dispersion and source location, *J. Geophys. Res.*, *114*, A06202, doi:10.1029/2008JA013549.

Bunch, N. L., M. Spasojevic, and Y. Y. Shprits (2011), On the latitudinal extent of chorus emissions as observed by the Polar Plasma Wave Instrument, *J. Geophys. Res.*, *116*, A04204, doi:10.1029/2010JA016181.

Burtis, W. J., and R. A. Helliwell (1969), Banded chorus—A new type of VLF radiation observed in the magnetosphere by OGO 1 and OGO 3, *J. Geophys. Res.*, *74*(11), 3002–3010, doi:10.1029/JA074i011p03002.

Burton, R. K., and R. E. Holzer (1974), The origin and propagation of chorus in the outer magnetosphere, *J. Geophys. Res.*, *79*(7), 1014–1023, doi:10.1029/JA079i007p01014.

Cattell, C., et al. (2008), Discovery of very large amplitude whistler-mode waves in Earth's radiation belts, *Geophys. Res. Lett.*, *35*, L01105, doi:10.1029/2007GL032009.

Chen, Y., G. D. Reeves, and R. H. W. Friedel (2007), The energization of relativistic electrons in the outer Van Allen radiation belt, *Nat. Phys.*, *3*, 614–617, doi:10.1038/nphys655.

Chum, J., O. Santolík, D. A. Gurnett, and J. S. Pickett (2009), Oblique lower band chorus waves: Time shifts between discrete elements observed by the Cluster spacecraft, *J. Geophys. Res.*, *114*, A00F02, doi:10.1029/2009JA014366.

Cully, C. M., J. W. Bonnell, and R. E. Ergun (2008a), THEMIS observations of long-lived regions of large-amplitude whistler waves in the inner magnetosphere, *Geophys. Res. Lett.*, *35*, L17S16, doi:10.1029/2008GL033643.

Cully, C. M., R. E. Ergun, K. Stevens, A. Nammari, and J. Westfall (2008b), The THEMIS digital fields board, *Space Sci. Rev.*, *141*(1–4), 343–355, doi:10.1007/s11214-008-9417-1.

Glauert, S. A., and R. B. Horne (2005), Calculation of pitch angle and energy diffusion coefficients with the PADIE code, *J. Geophys. Res.*, *110*, A04206, doi:10.1029/2004JA010851.

Goldstein, B. E., and B. T. Tsurutani (1984), Wave normal directions of chorus near the equatorial source region, *J. Geophys. Res.*, *89*(A5), 2789–2810, doi:10.1029/JA089iA05p02789.

Haque, N., M. Spasojevic, O. Santolík, and U. S. Inan (2010), Wave normal angles of magnetospheric chorus emissions observed on the Polar spacecraft, *J. Geophys. Res.*, *115*, A00F07, doi:10.1029/2009JA014717.

Hayakawa, M., Y. Yamanaka, M. Parrot, and F. Lefeuvre (1984), The wave normals of magnetospheric chorus emissions observed on board GEOS 2, *J. Geophys. Res.*, *89*(A5), 2811–2821, doi:10.1029/JA089iA05p02811.

Horne, R. B., and R. M. Thorne (2003), Relativistic electron acceleration and precipitation during resonant interactions with whistler-mode chorus, *Geophys. Res. Lett.*, *30*(10), 1527, doi:10.1029/2003GL016973.

Horne, R. B., et al. (2005a), Wave acceleration of electrons in the Van Allen radiation belts, *Nature*, *437*, 227–230, doi:10.1038/nature03939.

Horne, R. B., R. M. Thorne, S. A. Glauert, J. M. Albert, N. P. Meredith, and R. R. Anderson (2005b), Timescale for radiation belt electron acceleration by whistler mode chorus waves, *J. Geophys. Res.*, *110*, A03225, doi:10.1029/2004JA010811.

Hospodarsky, G. B., T. F. Averkamp, W. S. Kurth, D. A. Gurnett, M. Dougherty, U. Inan, and T. Wood (2001), Wave normal and Poynting vector calculations using the Cassini radio and plasma wave instrument, *J. Geophys. Res.*, *106*(A12), 30,253–30,269, doi:10.1029/2001JA900114.

Kennel, C. F., and H. E. Petschek (1966), Limit on stably trapped particle fluxes, *J. Geophys. Res.*, *71*(1), 1–28, doi:10.1029/JZ071i001p00001.

Koons, H. C., and J. L. Roeder (1990), A survey of equatorial magnetospheric wave activity between 5 and 8 RE, *Planet. Space Sci.*, *38*(10), 1335–1341, doi:10.1016/0032-0633(90)90136-E.

Lauben, D. S., U. S. Inan, T. F. Bell, and D. A. Gurnett (2002), Source characteristics of ELF/VLF chorus, *J. Geophys. Res.*, *107*(A12), 1429, doi:10.1029/2000JA003019.

Le Contel, O., et al. (2008), First results of the THEMIS search coil magnetometers, *Space Sci. Rev.*, *141*(1–4), 509–534, doi:10.1007/s11214-008-9371-y.

LeDocq, M. J., D. A. Gurnett, and G. B. Hospodarsky (1998), Chorus source locations from VLF Poynting flux measurements with the Polar spacecraft, *Geophys. Res. Lett.*, *25*(21), 4063–4066, doi:10.1029/1998GL900071.

Li, W., Y. Y. Shprits, and R. M. Thorne (2007), Dynamic evolution of energetic outer zone electrons due to wave-particle interactions during storms, *J. Geophys. Res.*, *112*, A10220, doi:10.1029/2007JA012368.

Li, W., R. M. Thorne, N. P. Meredith, R. B. Horne, J. Bortnik, Y. Y. Shprits, and B. Ni (2008), Evaluation of whistler mode chorus amplification during an injection event observed on CRRES, *J. Geophys. Res.*, *113*, A09210, doi:10.1029/2008JA013129.

Li, W., et al. (2009), Global distribution of whistler-mode chorus waves observed on the THEMIS spacecraft, *Geophys. Res. Lett.*, *36*, L09104, doi:10.1029/2009GL037595.

Li, W., R. M. Thorne, J. Bortnik, Y. Nishimura, V. Angelopoulos, L. Chen, J. P. McFadden, and J. W. Bonnell (2010a), Global distributions of suprathermal electrons observed on THEMIS and potential mechanisms for access into the plasmasphere, *J. Geophys. Res.*, *115*, A00J10, doi:10.1029/2010JA015687.

Li, W., et al. (2010b), THEMIS analysis of observed equatorial electron distributions responsible for the chorus excitation, *J. Geophys. Res.*, *115*, A00F11, doi:10.1029/2009JA014845.

Li, W., R. M. Thorne, J. Bortnik, Y. Y. Shprits, Y. Nishimura, V. Angelopoulos, C. Chaston, O. Le Contel, and J. W. Bonnell (2011), Typical properties of rising and falling tone chorus waves, *Geophys. Res. Lett.*, *38*, L14103, doi:10.1029/2011GL047925.

Lorentzen, K. R., J. B. Blake, U. S. Inan, and J. Bortnik (2001), Observations of relativistic electron microbursts in association with VLF chorus, *J. Geophys. Res.*, *106*(A4), 6017–6027, doi:10.1029/2000JA003018.

Macúšová, E., et al. (2010), Observations of the relationship between frequency sweep rates of chorus wave packets and plasma density, *J. Geophys. Res.*, *115*, A12257, doi:10.1029/2010JA015468.

Means, J. D. (1972), Use of the three-dimensional covariance matrix in analyzing the polarization properties of plane waves, *J. Geophys. Res.*, *77*(28), 5551–5559, doi:10.1029/JA077i028p05551.

Meredith, N. P., R. B. Horne, and R. R. Anderson (2001), Substorm dependence of chorus amplitudes: Implications for the acceleration of electrons to relativistic energies, *J. Geophys. Res.*, *106*(A7), 13,165–13,178, doi:10.1029/2000JA900156.

Meredith, N. P., R. B. Horne, R. M. Thorne, and R. R. Anderson (2003), Favored regions for chorus-driven electron acceleration to relativistic energies in the Earth's outer radiation belt, *Geophys. Res. Lett.*, *30*(16), 1871, doi:10.1029/2003GL017698.

Muto, H., M. Hayakawa, M. Parrot, and F. Lefeuvre (1987), Direction finding of half-gyrofrequency VLF emissions in the off-equatorial region of the magnetosphere and their generation and propagation, *J. Geophys. Res.*, *92*(A7), 7538–7550, doi:10.1029/JA092iA07p07538.

Roux, A., O. Le Contel, C. Coillot, A. Bouabdellah, B. de la Porte, D. Alison, S. Ruocco, and M. C. Vassal (2008), The search coil magnetometer for THEMIS, *Space Sci. Rev.*, *141*(1–4), 265–275, doi:10.1007/s11214-008-9455-8.

Santolík, O., D. A. Gurnett, J. S. Pickett, M. Parrot, and N. Cornilleau-Wehrlin (2003), Spatio-temporal structure of storm-time chorus, *J. Geophys. Res.*, *108*(A7), 1278, doi:10.1029/2002JA009791.

Santolík, O., E. Macúšová, K. H. Yearby, N. Cornilleau-Wehrlin, and H. StC. K. Alleyne (2005), Radial variation of whistler-mode chorus: First results from the STAFF/DWP instrument on board the Double Star TC-1 spacecraft, *Ann. Geophys.*, *23*, 2937–2942, doi:10.5194/angeo-23-2937-2005.

Santolík, O., E. Macúšová, E. E. Titova, B. V. Kozelov, D. A. Gurnett, J. S. Pickett, V. Y. Trakhtengerts, and A. G. Demekhov (2008), Frequencies of wave packets of whistler-mode chorus inside its source region: A case study, *Ann. Geophys.*, *26*, 1665–1670, doi:10.5194/angeo-26-1665-2008.

Santolík, O., D. A. Gurnett, J. S. Pickett, J. Chum, and N. Cornilleau-Wehrlin (2009), Oblique propagation of whistler mode waves in the chorus source region, *J. Geophys. Res.*, *114*, A00F03, doi:10.1029/2009JA014586.

Shprits, Y. Y., D. Subbotin, and B. Ni (2009), Evolution of electron fluxes in the outer radiation belt computed with the VERB code, *J. Geophys. Res.*, *114*, A11209, doi:10.1029/2008JA013784.

Tao, X., J. Bortnik, J. M. Albert, K. Liu, and R. M. Thorne (2011), Comparison of quasilinear diffusion coefficients for parallel propagating whistler mode waves with test particle simulations, *Geophys. Res. Lett.*, *38*, L06105, doi:10.1029/2011GL046787.

Thorne, R. M. (2010), Radiation belt dynamics: The importance of wave-particle interactions, *Geophys. Res. Lett.*, *37*, L22107, doi:10.1029/2010GL044990.

Thorne, R. M., and C. F. Kennel (1967), Quasi-trapped VLF propagation in the outer magnetosphere, *J. Geophys. Res.*, *72*(3), 857–870, doi:10.1029/JZ072i003p00857.

Thorne, R. M., T. P. O'Brien, Y. Y. Shprits, D. Summers, and R. B. Horne (2005), Timescale for MeV electron microburst loss during geomagnetic storms, *J. Geophys. Res.*, *110*, A09202, doi:10.1029/2004JA010882.

Tsurutani, B. T., and E. J. Smith (1974), Postmidnight chorus: A substorm phenomenon, *J. Geophys. Res.*, *79*(1), 118–127, doi:10.1029/JA079i001p00118.

Tsurutani, B. T., and E. J. Smith (1977), Two types of magnetospheric ELF chorus and their substorm dependences, *J. Geophys. Res.*, *82*(32), 5112–5128, doi:10.1029/JA082i032p05112.

Tsurutani, B. T., O. P. Verkhoglyadova, G. S. Lakhina, and S. Yagitani (2009), Properties of dayside outer zone chorus during HILDCAA events: Loss of energetic electrons, *J. Geophys. Res.*, *114*, A03207, doi:10.1029/2008JA013353.

V. Angelopoulos, Department of Earth and Space Sciences, Institute of Geophysics and Planetary Physics, University of California at Los Angeles, CA 90095-1567, USA.

J. Bortnik, W. Li, and R. M. Thorne, Department of Atmospheric and Oceanic Sciences, University of California at Los Angeles, 405 Hilgard Avenue, Los Angeles, CA 90095-1565, USA. (moonli@atmos.ucla.edu)